

# Enhancing Performance and Function of Polymethacrylate Extreme Ultraviolet Resists using Area-Selective Deposition

*Rachel A. Nye,<sup>1,2,3</sup> Kaat Van Dongen,<sup>1,2</sup> Danilo De Simone,<sup>1</sup> Hironori Oka,<sup>1,4</sup> Gregory N. Parsons,<sup>3</sup> Annelies Delabie<sup>1,2,\*</sup>*

<sup>1</sup> IMEC, Kapeldreef 75, Leuven, Belgium, 3001

<sup>2</sup> KU Leuven (University of Leuven), Leuven, Belgium, 3001

<sup>3</sup> North Carolina State University, Department of Chemical and Biomolecular Engineering, 911 Partners Way, Raleigh, USA, 27606

<sup>4</sup> FUJIFILM Corporation Electronic Materials Research Laboratories, Kawashiri 4000, Yoshida-Cho, Haibara-Gun, Shizuoka, Japan

**ABSTRACT:** Extreme ultraviolet (EUV) lithography is a critical enabler in next-generation technology, although the low etch resistance of conventional organic EUV resists results in low resolution pattern transfer, particularly for smaller features. In this work, we integrate area-selective deposition (ASD), a bottom-up nanopatterning technique, with EUV resists of industrially relevant thicknesses (<50 nm thick) to form resist hardening or tone inverting layers for improved resolution. We utilize TiO<sub>2</sub> ASD via atomic layer deposition on 25-35 nm thin photosensitive polymethacrylate-based EUV materials. By tuning the polymer structure and

functionality, we enable different scenarios for selective deposition on top of the resist, infiltrated into the bulk resist, or selective to the resist. We find that a cyclohexyl protecting group causes TiO<sub>2</sub> inhibition, thus showing promise for tone inversion applications with oxide underlayers. In contrast, resist materials containing a *tert*-butyl protecting group are good candidates for resist hardening because they enable TiO<sub>2</sub> deposition on both EUV exposed and unexposed polymers. Furthermore, we report the integration of a dimethylamino-trimethylsilane inhibitor with the resists to inhibit TiO<sub>2</sub> surface nucleation and facilitate sub-surface diffusion, thus further broadening potential applications. The results described here establish an important baseline for utilizing ASD on various organic resists to achieve tone inversion or resist hardening and hence improve EUV pattern resolution.

## INTRODUCTION

As next-generation technology nodes (< 7 nm) continue to push the limits of Moore's Law,<sup>1,2</sup> manufacturing requirements are outpacing the capabilities of conventional 193 nm ArF lithography. Advanced techniques such as immersion lithography or self-aligned double and quadruple patterning (SADP/SAQP) can further reduce feature size, but they also increase manufacturing complexity and cost.<sup>3,4</sup> Shorter wavelengths of light, such as that used by extreme ultraviolet lithography (EUVL,  $\lambda = 13.5$  nm), provide an effective method to achieve smaller pattern dimensions without the increase in cost and complexity associated with multi-patterning techniques.<sup>4-9</sup> While EUVL has already demonstrated sub-20 nm patterns,<sup>4,10-12</sup> new resist materials and processes are needed that simultaneously meet the qualifications for resolution, line-edge roughness (LER), and sensitivity.<sup>5,13-17</sup>

Current photoresists are typically polymer-based chemically amplified resists (CARs)<sup>18</sup> with a photoacid generator (PAG) to catalyze deprotection of the polymers after EUV exposure.<sup>3,17</sup> While CARs have already demonstrated promising results for 12 nm half-pitch and potential for the 7 nm node,<sup>19,20</sup> they suffer from low etch resistance and risk of pattern collapse.<sup>21,22</sup> Thinner resist layers mitigate pattern collapse<sup>23</sup> but typically result in poor etch selectivity to underlying layers, especially when resist is <50 nm thick.<sup>5,16,24,25</sup> Moreover, the polymeric properties (such as glassy transition temperature ( $T_g$ ) and modulus, which are important factors in determining polymer behavior and applications) can depend on thickness, so that performance degrades as thickness decreases.<sup>17,26–29</sup> Therefore, a means to improve performance of thin resist layers is particularly important for advanced EUV applications.

Area-selective deposition (ASD) presents several innovative ways to improve resolution, etch resistance, pattern collapse, and defect repair in EUV lithography.<sup>30</sup> ASD is a bottom-up patterning technique using vapor-solid surface reactions to deposit thin films on a desired growth surface with minimal effect on adjacent non-growth regions.<sup>31–33</sup> As shown schematically in Figure 1, two scenarios we explore to integrate ASD with EUVL are tone inversion and resist hardening. Furthermore, two options we consider for resist hardening include coating by ASD and selective reactant infiltration.

Figure 1a shows production of a positive-tone image by EUV resist exposure, where the EUV exposed region is removed during development. Positive-tone organic resists are common in EUV lithography because they are relatively easy to synthesize. Figure 1b demonstrates a “tone-inversion” process, which converts a positive image (printed with positive resist) to a negative image. Tone-inversion via ASD is interesting because it uses a relatively simple positive resist material to produce a negative image, where the resulting imaged material is more etch resistant

than most available starting organic resist materials.<sup>3,15,34,35</sup> For ideal tone-inversion ASD, it is desirable for the film to nucleate rapidly on the underlying substrate with minimal growth on the developed resist.

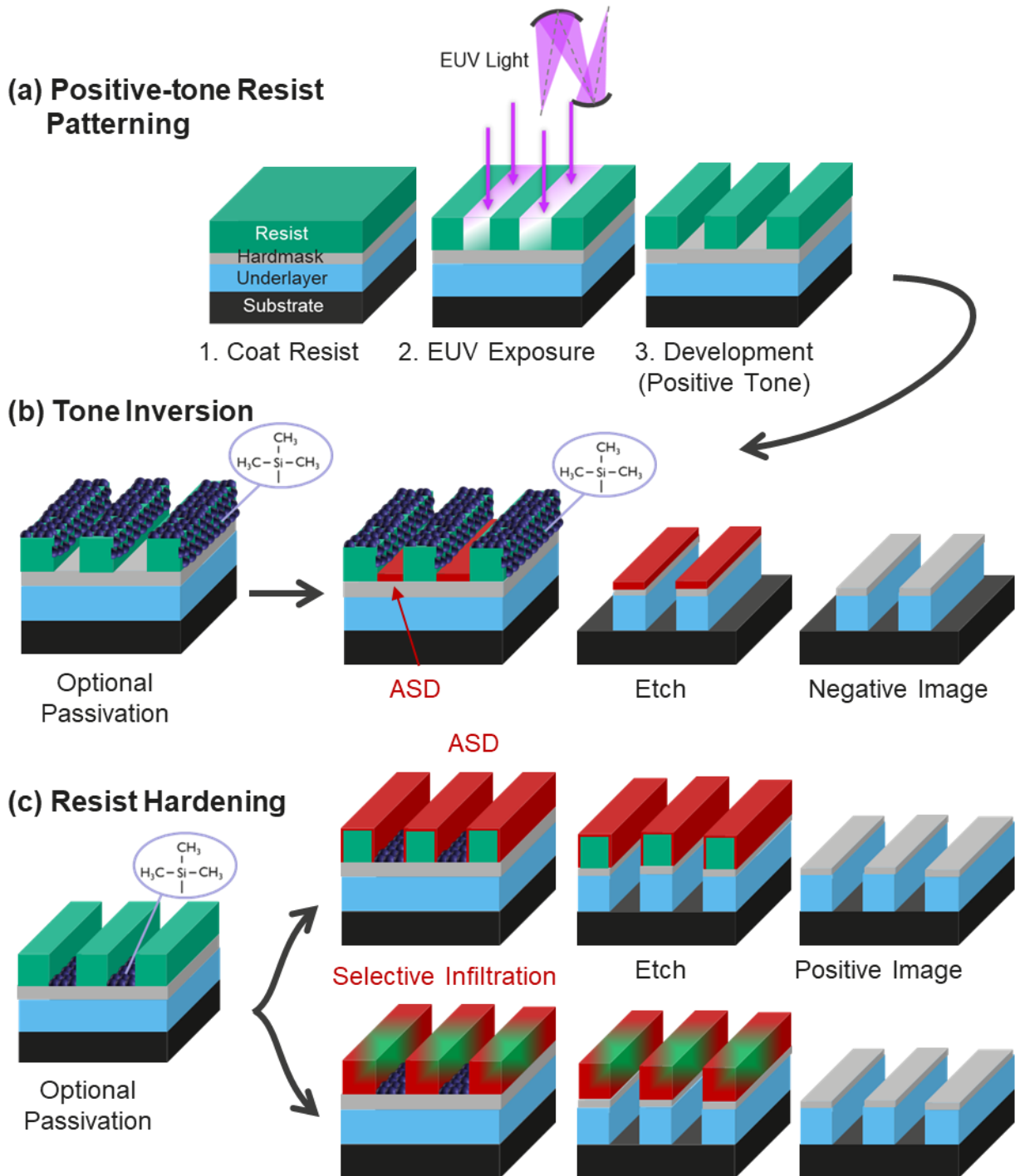


**Figure 1.** Schematic of (a) positive tone EUV resist exposure and possible interactions between a positive-tone EUV resist and ASD: (b) tone inversion from ASD on the substrate selective to the resist, or (c) resist hardening from ASD on the resist selective to the substrate. Tone inversion and resist hardening may optionally be facilitated with a passivation step, such as from a small molecule inhibitor.

Figure 1c demonstrates EUV pattern improvement via resist-hardening. In this scenario, the patterned resist is modified to improve etch resistance and mitigate pattern collapse, thereby enabling the use of thin resist materials.<sup>6,36-38</sup> For example, metal oxides have demonstrated higher etch resistance than traditional organic resists, and are a good candidate for resist hardening applications.<sup>5,24,25</sup> As shown in Figure 1c, two approaches for resist hardening include ASD of an etch resistant layer on a patterned resist (in which case the resist serves as the growth surface and rapid nucleation is desirable),<sup>30,37</sup> and selective reactant infiltration into the patterned resist (which takes advantage of small precursors selectively diffusing into a polymer).<sup>39-41</sup> In either case, the reaction can proceed on the as-prepared resist pattern, or after exposure to a nucleation inhibitor.<sup>6,42,43</sup> The selective infiltration approach introduces a metal oxide into the resist, and may have the additional benefit of not substantially affecting the pattern critical dimension (CD).<sup>26</sup>

As shown in Figure 1, the inhibition for both tone inversion and resist hardening could be achieved via an inherent delay on the clean surface, or by using a passivating molecule such as a small-molecule inhibitor (SMI) that selectively adsorbs on the desired non-growth substrate. A SMI of interest in this work is such as N,N-dimethylamino-trimethylsilane (DMA-TMS) which can chemisorb onto available surface -OH sites to form passivating -O-Si(CH<sub>3</sub>)<sub>3</sub> groups:<sup>44,45</sup>



DMA-TMS could enhance resist hardening by passivating and blocking ALD on exposed SiO<sub>2</sub> while allowing coating or infiltration into the patterned resist. Likewise, DMA-TMS could promote tone inversion by passivating the resist surface, allowing selective growth on the exposed substrate region.

Despite these possible advantages, there are few reports of ASD integration with EUV materials and processes.<sup>37,46</sup> A key problem to date is that when the resist thickness is reduced to industrially relevant values (i.e. < 50 nm), the ability to integrate the resist into a successful ASD process is substantially diminished.<sup>40,46–49</sup> One possible solution is to incorporate inhibitors such as DMA-TMS to passivate the starting substrate material. Another key consideration for integrated ASD-EUV is that the process temperature required for ASD must be low enough, typically  $\lesssim 200^{\circ}\text{C}$ , to maintain the chemical integrity of the resist.<sup>33</sup> Thus, additional research effort is needed to facilitate ASD integration with thin, (i.e. <50 nm) commercially relevant resist layers.<sup>30</sup>

In this work, we report area-selective deposition of TiO<sub>2</sub> via atomic layer deposition (ALD) on a wide range of thin (< 35 nm) photosensitive polymethacrylate EUV resist materials. The resist materials studied here have a range of backbone and pendant groups specifically designed for the ASD scenarios shown in Figure 1. TiO<sub>2</sub> ALD is selective to many materials<sup>32,36,50</sup> and has favorable chemical stability, etch resistance,<sup>42,51</sup> and low deposition temperature.<sup>6,52</sup> We begin by evaluating the surface properties of all the resists, including how the properties are affected by EUV exposure, DMA-TMS treatment, and TiO<sub>2</sub> ALD. We show that treating the polymers with DMA-TMS can help passivate TiO<sub>2</sub> ALD on the surface while enabling sub-surface Ti infiltration.<sup>53</sup> Additionally, we describe mechanisms for selectivity loss, in particular how different protecting groups in the methacrylate polymer influence ALD nucleation. The results obtained here contribute relevant

examples of thin EUV resist materials that can be integrated with TiO<sub>2</sub> ASD for both tone inversion and resist hardening applications, and are expected to lead to improvements in EUV pattern resolution.

## EXPERIMENTAL

### A. Spin-Coating, EUV Exposure, and Development

Resist materials, including polymers and PAG, were provided by Fujifilm and used as received. Polymers were chosen to explore a range of protecting groups, surface terminations, and glassy transition temperatures.<sup>17</sup> Substrates consisted of 300 mm silicon wafers with native oxide (referred to throughout the text as SiO<sub>2</sub> wafers). Polymers were spin-coated ~30 nm thick onto silicon substrates in an NXE:3300B track. The spin-coating process began with a 30 s priming step at 135 °C to form a < 1 nm thick HMDS layer on the Si surface to improve polymer adhesion. The polymer resist was then spin-coated for 30 s at a speed between 1000 – 1500 revolutions per minute (RPMs) depending on the polymer. A post-apply bake (PAB) was conducted at 120 °C for 90 s. The wafers were then exposed to EUV light at 15 mJ/cm<sup>2</sup> in an ASML full-field NXE:3300B scanner. Five regions of 32 mm by 26 mm in a line across the center of the 300 mm wafer were exposed. A post-exposure bake (PEB) was conducted at 120 °C for 90 s. In some experiments, a development step was used for the positive-tone resist in tetramethyl-ammonium hydroxide solution (0.26 Normality). After the PEB (or development step if applicable), wafers were cleaved into coupons based on EUV exposure status for further experiments. In our previous work<sup>54</sup> we demonstrated minimal change to surface WCA for unexposed resist regions before and after development. Therefore, in this study, the unexposed resist regions without development are used

to represent unexposed regions after the full lithographic process (i.e. including development). Future work should confirm the ASD behavior on resist materials including the development step.

#### B. TiO<sub>2</sub> Atomic Layer Deposition and DMA-TMS Treatment

Thermal stability at the ALD temperature (125 °C) was confirmed by verifying consistent surface hydrophobicity (with WCA measurements) and surface roughness (with AFM measurements) before and after annealing. Annealing was performed by cleaving polymer-coated wafers into coupons and placing them in an oven under lab air ambient environment at 135 °C for 60 minutes. TiO<sub>2</sub> ALD was performed in a Polygon 8300 EmerALD chamber at 125 °C at a pressure of 5 Torr using TiCl<sub>4</sub> and H<sub>2</sub>O with a recipe that demonstrated well-saturated ALD behavior, described previously.<sup>36</sup> Wafers were degassed for 1 minute before deposition started. Growth rate on SiO<sub>2</sub> at these conditions was ~0.037 nm/cycle. SiO<sub>2</sub> and polymer surfaces were passivated with DMA-TMS at 135, 180, and 250 °C. Passivation times varied between 300-1140 s. DMA-TMS passivation took place in a TEL Tactras chamber at 5 Torr in a N<sub>2</sub> environment, with details described previously.<sup>36</sup>

#### C. Characterization

Polymer thickness was confirmed before and after EUV exposure and development with spectroscopic ellipsometry (SE) for 5 points on a KLA Tencor F5-SCD spectroscopic ellipsometer. WCA measurements were performed on a Dataphysics OCAH 230 tool using 1 mL deionized water droplets. Reported values are the average of five measurements on one sample, with the standard deviation used as the error. Atomic force microscopy (AFM) was performed with a Bruker Dimension Edge instrument in tapping mode with ScanAsyst using a 300 kHz tip. Scan sizes were 1 μm<sup>2</sup>.

Titanium content on the resist surfaces was quantified with Rutherford backscattering spectrometry (RBS) using a 1.523 MeV He<sup>+</sup> incoming ion beam. From the measured aerial density of Ti, the equivalent TiO<sub>2</sub> thickness is calculated using a TiO<sub>2</sub> density of 3.72 g/cm<sup>3</sup>. X-ray photoelectron spectroscopy (XPS) was used to analyze surface chemistry after passivation and etching. This was conducted using a Thermo Scientific Theta 300 instrument with a 1486.6 eV monochromatized Al K $\alpha$  X-ray source with a 400  $\mu$ m spot size. Each XPS scan was calibrated to the C 1s peak at 284.8 eV. Transmission electron microscopy (TEM) and energy dispersive x-ray spectroscopy (EDS) were performed on a Tecnai F30 ST (FEI) tool with an FEG electron source at 300 kV. Prior to TEM imaging, samples were prepared with a dual beam FIB/SEM Nova600i (FEI) and Ar Ion miller PIPS (Gatan). Time-of-flight secondary ion mass spectrometry (ToF-SIMS) was performed on a TOFSIMS V tool from ION-TOF GmbH.

## RESULTS AND DISCUSSION

### A. EUV (Co)polymers and Their Surface Properties

In this work, we selected a wide range of stable resist materials shown in Figure 2, including homopolymers PtBuMA, PCHMA, PMCPMA, and PHS, as well as random block co-polymers, P(NLMA-r-CHMA), P(NLMA-r-MCPMA) and P(HS-r-tBuMA), and studied them both with and without the addition of 4-(methylphenyl) triphenyl sulfonium nonaflate as a photo-acid generator (PAG, structure shown in Figure S1). For each material, the properties and extent of ALD nucleation were evaluated in the as-spun condition and after blanket EUV exposure. For the experiments, Si wafers were primed with hexamethylenedisilazane (HMDS) and the polymers were spin-coated to a thickness of  $\sim$ 35 nm, as confirmed by ellipsometry, then cleaved into coupons ( $\sim$ 2 in x 2 in). Some of the samples were then exposed to 15 mJ/cm<sup>2</sup> EUV light. Samples

are characterized by water contact angle, ellipsometry to obtain film thickness, and X-ray photoelectron spectroscopy (XPS) to determine composition. Results are shown in Figure 2, Figure S2 and Table S1.

As shown in Figure 2, in the as-spun condition, the water contact angle data indicates all polymers are hydrophobic. The co-polymers are somewhat less hydrophobic compared to the methacrylate homopolymers with protecting groups (i.e. PtBuMA, PCHMA, and PMCPMA), consistent with the presence of more O or OH groups. Similarly, PHS (with the highest concentration of surface OH groups) demonstrates the least hydrophobicity. The addition of a small amount of PAG does not significantly affect WCA, indicating that the WCA is primarily determined by the polymer backbone. For each polymer + PAG material, exposure to EUV leads to a decrease in film thickness from 35 to ~26 nm. For the PtBuMA + PAG sample, the surface became more hydrophilic after EUV treatment, and XPS results (Figure S2 and Table S1) show an increase in C=O bonds relative to C-O, consistent with conversion from tBu to hydrophilic -OH groups (i.e. deprotection).<sup>54-56</sup> We note that for the polymers without PAG, EUV exposure did not significantly affect WCA (data not shown), as without PAG the polymer deprotection reaction occurs to a much lesser extent, leaving hydrophobic tBu protecting groups as the predominant surface groups.<sup>54,57,58</sup> These trends in surface hydrophobicity (determined by the polymer protecting groups) can indicate the potential for nucleation inhibition during TiO<sub>2</sub> ALD, where more hydrophobic surfaces are expected to have a longer nucleation delay.<sup>44,45,59</sup>

Thermal stability of the starting materials was analyzed by measuring WCA and RMS roughness for samples in the as-prepared condition, and after heating to 135 °C for 60 min (consistent with the expected ALD process time) under N<sub>2</sub> ambient. Results in Figure S3 and S4, respectively, demonstrate materials remain stable upon extended thermal treatment.<sup>30</sup>

Polymer		PtBuMA	PCHMA	PMCPMA	P(NLMA-r-CHMA)	P(NLMA-r-MCPMA)	P(HS-r-tBuMA)	PHS
Structure								
Static WCA (°)	Polymer Only	88	86	85	83	82	76	61
	Polymer with PAG	82	-	-	-	-	72	64
	Polymer with PAG and EUV exposure	33	-	-	-	-	61	61

**Figure 2.** Chemical structures and WCAs of each polymer material utilized in this work. WCAs are measured as-spin coated without PAG, with PAG, and with PAG after EUV exposure and post-exposure bake. PtBuMA: poly(tert-butyl methacrylate); PCHMA: poly(cyclohexyl methacrylate); PMCPMA: poly(1-methylcyclopentyl methacrylate); P(NLMA-r-CHMA): poly(2-oxohexahydro-6aH-3,5-methanocyclopenta[b]furan-6a-yl 2,2-dimethylbutanoate-random-cyclohexyl methacrylate); P(NLMA-r-MCPMA): poly(2-oxohexahydro-6aH-3,5-methanocyclopenta[b]furan-6a-yl 2,2-dimethylbutanoate-random-1-methylcyclopentyl methacrylate); P(HS-r-tBuMA): poly(p-hydroxystyrene-random-tert-butyl methacrylate); PHS: poly(p-hydroxystyrene); Photo-acid generator (PAG): 4-(methylphenyl) triphenyl sulfonium nonaflate (structure shown in Figure S1).

## B. TiO<sub>2</sub> ALD on Polymers with Various Protecting Groups

### 3.B.1. TiO<sub>2</sub> ALD on Various Polymer Surfaces

To analyze TiO<sub>2</sub> nucleation, resist samples were treated with 0 to 300 cycles of TiO<sub>2</sub> ALD at 125 °C using TiCl<sub>4</sub> and H<sub>2</sub>O under continuous N<sub>2</sub> flow at 5 Torr.<sup>45</sup> Resulting RBS and WCA data is shown in Figure 3. The Ti aerial density measured by RBS is converted to an equivalent TiO<sub>2</sub>

layer thickness using a  $\text{TiO}_2$  density of  $3.72 \text{ g cm}^{-3}$ . Results for  $\text{TiO}_2$  ALD at  $150 \text{ }^\circ\text{C}$  on  $\text{SiO}_2$  and  $\text{SiO}_2$  exposed to DMA-TMS are also included in the plots. In Figure 3a, for  $\text{TiO}_2$  ALD on  $\text{SiO}_2$ , RBS results show that thickness increases linearly with ALD cycles, consistent with a growth per cycle of  $\sim 0.037 \text{ nm/cycle}$ .<sup>32,45,50,54,57,60</sup> For ALD on  $\text{SiO}_2$  treated with DMA-TMS,  $\text{TiO}_2$  is detected after  $\sim 100$  ALD cycles (equivalent thickness  $\sim 0.5 \text{ nm}$ ), indicating surface passivation and inhibited nucleation.<sup>45</sup> As also shown in Figure 3a, inhibited  $\text{TiO}_2$  nucleation is also observed on as-prepared P(NLMA-r-CHMA) and PCHMA polymers. For the other polymers, Figure 3b shows facile  $\text{TiO}_2$  nucleation and linear growth,<sup>36,48</sup> with thickness per cycle the same as on  $\text{SiO}_2$ .

During  $\text{TiO}_2$  ALD, nucleation is expected to occur when the  $\text{TiCl}_4$  precursor reacts with available surface -OH sites. Therefore, a hydrophobic surface with few available -OH sites will likely inhibit nucleation. Moreover, for a relatively thick ALD  $\text{TiO}_2$  film on  $\text{SiO}_2$ , the WCA is smaller than that on polymers. Therefore, as ALD proceeds on a hydrophobic resist, a decrease in WCA could correlate with the formation of  $\text{TiO}_2$  nuclei.<sup>48,61</sup> Figure 3c and d show the measured WCA vs ALD cycle for the materials studied. For  $\text{TiO}_2$  on  $\text{SiO}_2 + \text{DMA-TMS}$ , P(NLMA-r-CHMA) and PCHMA polymers, Figure 3c shows a relatively slow change in WCA during the first 100 ALD cycles, consistent with inhibited nucleation in Figure 3a. Note that for the  $\text{SiO}_2$  DMA-TMS surface, the high WCA indicates that the DMA-TMS inhibitor remains on the surface after 100 ALD cycles, as discussed previously.<sup>44,45</sup> For the other polymers, Figure 3d shows a rapid drop in WCA, consistent with rapid  $\text{TiO}_2$  nucleation. Similar experiments were conducted on polymers with PAG after EUV exposure and demonstrated similar  $\text{TiO}_2$  growth rates and WCAs, as shown in Figure S5.

To achieve tone-inversion (e.g. as shown in Figure 1b), utilizing resist materials that show an inherent delay in ALD nucleation would be most favorable.<sup>54,57</sup> Accordingly, for the polymers

studied here, the PCHMA and P(NLMA-r-CHMA) show the most favorable results. On PCHMA, 100 ALD cycles lead to only ~0.5 nm of TiO<sub>2</sub> (from RBS, Figure 3a), and the WCA remains >86° (Figure 3b). Likewise, on P(NLMA-r-CHMA), 100 ALD cycles produces < 0.6 nm of TiO<sub>2</sub>.

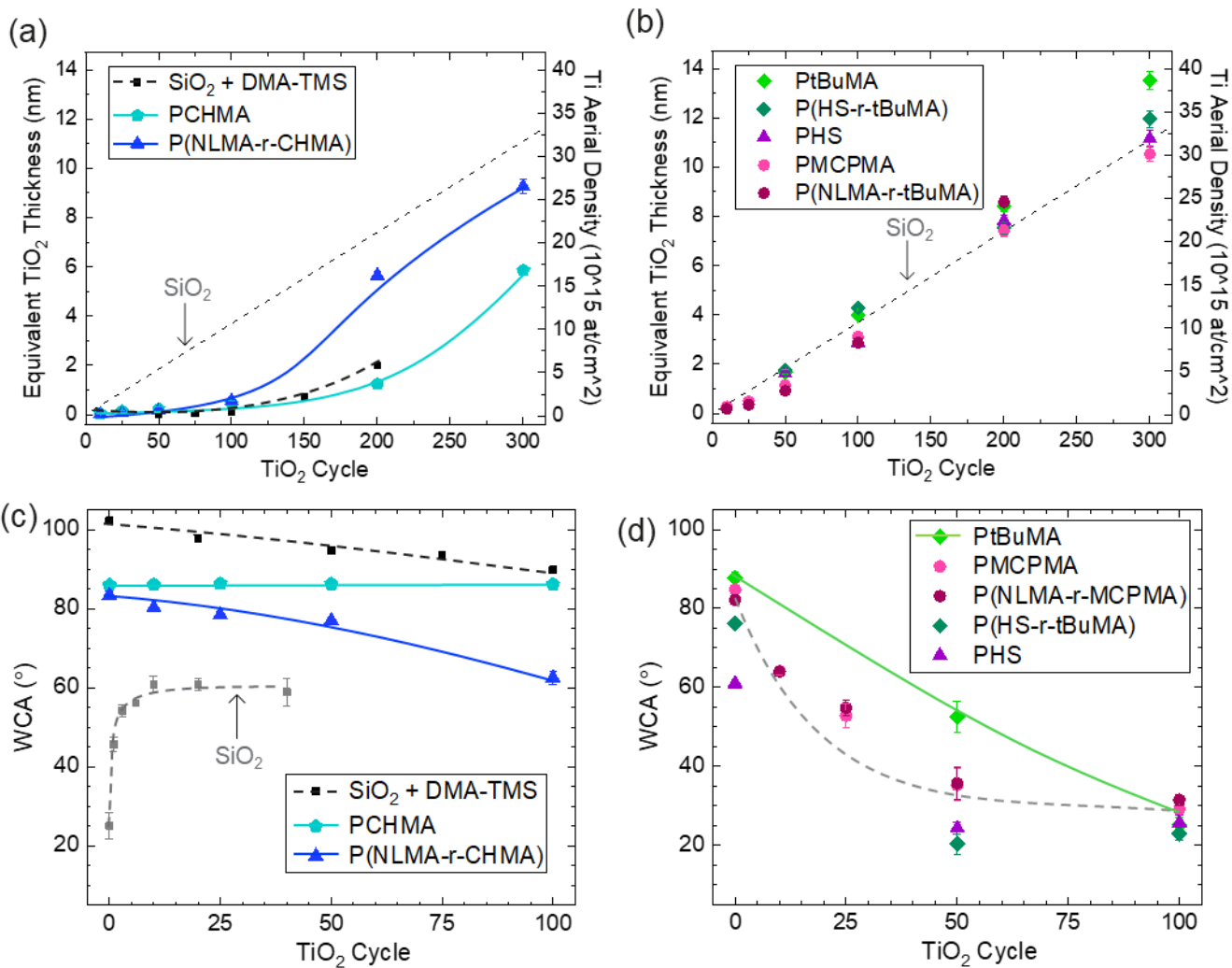


**Figure 3.** (a), (b) RBS (showing Ti aerial density on right y-axis and theoretical TiO<sub>2</sub> thickness on left y-axis) and (c), (d) WCA measurements for PCHMA (light blue squares), P(NLMA-r-CHMA) (dark blue squares), PMCPMA (light pink circles), P(NLMA-r-MCPMA) (dark pink circles), PHS (purple triangles), PtBuMA (light green diamonds), and P(HS-r-tBuMA) (dark green diamonds).

Data on SiO<sub>2</sub> and DMA-TMS passivated SiO<sub>2</sub> are included, as indicated on the Figure, as a reference growth and non-growth surface, respectively. Lines are drawn as guides to the eye.

Close examination of the trends in Figure 3 reveals that TiO<sub>2</sub> nucleation does not necessarily correlate directly with surface hydrophobicity, but rather appears to depend on the functionality of the pendant group. (WCA is sometimes used as a convenient initial indicator for selectivity as most ASD processes nucleate more slowly on hydrophobic surfaces compared to hydrophilic hydroxyl terminated surfaces).<sup>45,62</sup> For example, comparing nucleation on PMCPMA and PCHMA homopolymers, growth proceeds readily on PMCPMA but not on PCHMA, even though the initial WCA (85-86 °) and the size of the protecting group (i.e., number of C atoms) is similar for both materials. A key difference between these polymers is that on PCHMA, the ester group is linked to the cyclic protective moiety via a secondary carbon, whereas for PMCPMA, the link is through a tertiary carbon. Therefore, the nature of the protective group and linkage may be important in controlling nucleation. Another interesting result is that compared to PHS or P(HS-r-tBuMA) polymers, growth proceeds more quickly on the more hydrophobic PtBuMA. We hypothesize that in this case, the TiCl<sub>4</sub> precursor can diffuse more readily into the bulk of the PtBuMA. The effect of reactant diffusion into the polymers during ALD is discussed in more detail in the following section.

### *3.B.2. Interactions Between TiCl<sub>4</sub> Precursor and Polymer Surfaces and/or Bulk*

To differentiate between resist hardening by ASD and resist hardening by selective infiltration (Fig. 1c), we also explore TiO<sub>2</sub> precursor diffusion into the polymer bulk. For this test, seven sample pieces, including PHS, PtBuMA, and P(HS-r-tBuMA) with and without PAG, as well as a

PtBuMA + PAG sample after EUV exposure, are placed in the ALD reactor and exposed to  $\text{TiCl}_4$  (without water doses), using otherwise the same conditions used for ALD. After either a single dose or 10 sequential doses, samples are removed from the reactor and analyzed by RBS and XPS, and results are shown in Figure 4 and Table S2, respectively.

As shown in Figure 4, after 1 dose of  $\text{TiCl}_4$ , the Ti density was  $0.3\text{-}0.4 \times 10^{15}/\text{cm}^2$  for all materials studied. After 10 doses, the Ti content in the PHS and P(HS-r-tBuMA) materials remained approximately constant. This is consistent with the relatively large -OH density in these polymers, so that during the first dose, the  $\text{TiCl}_4$  can react near the surface to form Ti-O and possibly Ti-O-Ti linkages that can block sub-surface diffusion. However, for PtBuMA (with and without PAG) the additional nine doses of  $\text{TiCl}_4$  led to a marked increase in Ti content. We ascribe this difference to the smaller density of -OH groups in the PtBuMA, so that the  $\text{TiCl}_4$  tends to not react on the surface, but instead it can diffuse and react with available groups throughout the polymer bulk. The trend observed by RBS is corroborated by the atomic concentration values in Table S2 obtained from XPS. For the PtBuMA polymer, ToF-SIMS depth profile data collected before and after 100 cycles of  $\text{TiO}_2$  ALD (Figure S6) further confirms sub-surface titanium diffusion.

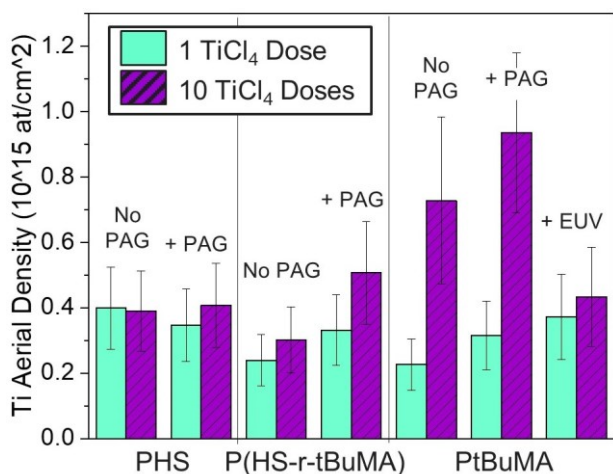


**Figure 4.** RBS measurements after one (green solid fill) and ten (purple striped fill) repeated  $\text{TiCl}_4$  doses on various surfaces. For each polymer (PHS, P(HS-r-tBuMA), and PtBuMA) results are

shown for samples with and without PAG, as indicated on the Figure. For PtBuMA + PAG, results are also shown after EUV exposure.

To explore the effect of polymer modification on the extent of precursor diffusion during ALD, we hypothesized that sub-surface reactant diffusion could be enhanced by blocking available reactive sites near the growth surface. For this test, we selected the PHS + PAG polymer which, as shown in Figures 3 and 4, allows rapid TiO<sub>2</sub> nucleation during ALD. Two samples of 30 nm PHS + PAG were prepared, and one was exposed to DMA-TMS for 300 s to react with and passivate accessible -OH sites. Then, both samples were placed in the ALD reactor and exposed to 100 cycles of ALD. After deposition, samples were analyzed by cross-section transmission electron microscopy (TEM) with elemental analysis from energy dispersive spectroscopy (EDS), and the resulting images are given in Figure 5 and S7.

For the as-prepared PHS + PAG, the image (5a) and Ti EDS signal (5b) indicate a distinct uniform ~4 nm TiO<sub>2</sub> film on top of the polymer. In contrast, for the PHS exposed to DMA-TMS, no surface TiO<sub>2</sub> film is observed (5c), and the Ti EDS signal (5d) is distributed uniformly throughout the bulk of the polymer. We note the swelling of the resist material treated with DMA-TMS and TiO<sub>2</sub> ALD from ~25 to ~47 nm thick, which is attributed to diffusion of the DMA-TMS inhibitor and/or the TiCl<sub>4</sub> precursor. One potential way to reduce swelling (and thereby reduce its impact on CD in patterns) would be to decrease the DMA-TMS treatment time and/or reduce the number of ALD cycles, and warrants future investigation.

These results are also observed from depth profiling of EDS line-scans, as in Figure 5e. Figure 5e shows a sharp Ti peak at the surface of the polymer layer for the sample without DMA-TMS inhibitor, whereas the Ti signal is dispersed throughout the polymer layer for the sample exposed to DMA-TMS. Additionally, the DMA-TMS treated polymer shows increased Si content within

the polymer layer compared to the polymer without DMA-TMS, suggesting that some of the DMA-TMS inhibitor also diffuses into the polymer. Therefore, modifying the available reactive groups prior to ALD treatment can be used to adjust the extent of Ti infiltration into polymer resists for resist-hardening applications, as shown in Figure 1c.

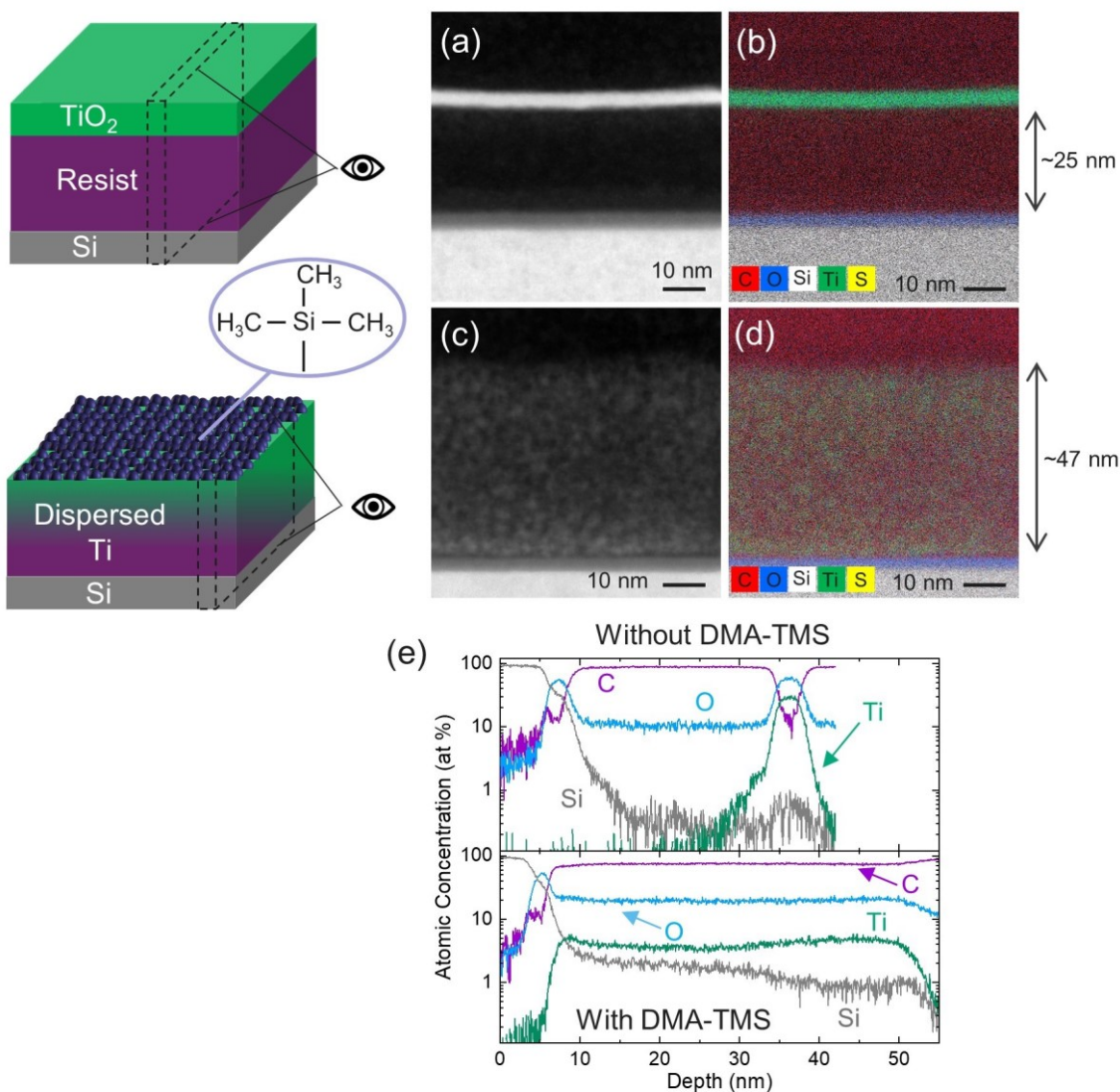


**Figure 5.** TEM high-angle annular dark-field (HAADF) (a,c) and EDS (b,d) images of 100 cycles TiO<sub>2</sub> deposited at 125 °C on (a-b) PHS + PAG and (c-d) DMA-TMS treated PHS + PAG. Elemental depth profiles are shown in (e). Color scheme for EDS maps are as follows: Ti (green), O (blue), C (red), S (yellow), Si (white).

## C. TiO<sub>2</sub> ALD on DMA-TMS Passivated Polymers

### *3.C.1. Effect of DMA-TMS Inhibitor on EUV Resist Materials*

To further explore ASD for resist hardening and tone inversion shown in Figure 1, we tested ALD nucleation on the starting substrate materials and on resist polymers after exposing them to dimethylamino-trimethylsilane (DMA-TMS). To test these processes, five sample pieces, including SiO<sub>2</sub> on Si, ~30 nm films of PHS + PAG and P(HS-r-tBuMA) + PAG, and PHS + PAG and P(HS-r-tBuMA) + PAG films exposed to 15 mJ/cm<sup>2</sup> of EUV, were placed in the reactor and dosed with DMA-TMS vapor at 135 °C for either 300 or 1140 s. The WCA on each surface before and after DMA-TMS treatment is given in Figure 6. For all samples, 300 s exposure to DMA-TMS increases the WCA to ~85-95°. Compared to the P(HS-r-tBuMA), the PHS contains a larger fraction of -OH groups, consistent with a somewhat larger WCA for PHS after DMA-TMS exposure. EUV exposed samples showed a similar change in WCA. The longer DMA-TMS treatment times do not significantly increase surface hydrophobicity, but they could affect the extent of diffusion into the polymer bulk. A fixed DMA-TMS exposure time of 300 s is maintained for further experiments.

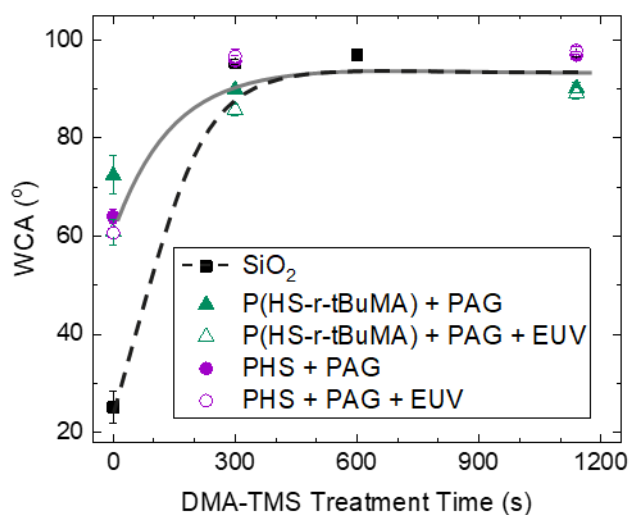


**Figure 6.** WCA measurements for various DMA-TMS treatment times at 135 °C on SiO<sub>2</sub> (black), PHS + PAG (purple) and P(HS-r-tBuMA) + PAG (green). Results are shown for treatment on both EUV exposed (dashed lines) and unexposed (solid lines) polymers.

### 3.C.2. TiO<sub>2</sub> ALD on EUV Resist Materials With and Without DMA-TMS Inhibitor

To test integration of DMA-TMS into ASD processes using resist materials, several approaches were tested including: 1) treating the initial SiO<sub>2</sub> substrate with DMA-TMS before resist coating; 2) treating as-spun resists with DMA-TMS before patterning with EUV; 3) treating patterned resist/SiO<sub>2</sub> surface with DMA-TMS. We note that for different material sets, different scenarios for integrating exposure, ASD (with optional inhibitor), and development may provide the highest selectivity, and should be considered when expanding these results to new materials. In this case, for the first approach, DMA-TMS on SiO<sub>2</sub> negatively impacted the subsequent resist coating. The second method also produced unfavorable results because the development step after EUV treatment tended to remove the DMA-TMS passivation from the resist surface (details described in SI).

To test the third approach, we prepared four sets of polymer samples: P(HS-r-tBuMA) + PAG, P(HS-r-tBuMA) + PAG + EUV, PHS + PAG, and PHS + PAG + EUV. One sample of each type was used as-prepared, and one sample of each type was exposed to DMA-TMS. Then, the eight sample pieces were transferred to the ALD reactor and coated with 50 cycles of TiO<sub>2</sub> at 125°C. Three additional sets of eight identical pieces were also prepared, and they were coated with 100, 200, and 300 cycles of ALD, respectively. After coating, all samples were analyzed by RBS and WCA. Results for samples without EUV treatment are shown in Figure 7, and those with EUV are given in S5.

The results in Figure 7 show that TiO<sub>2</sub> nucleates and grows readily on both polymers, the growth was similar with or without the DMA-TMS treatment. However, for PHS + PAG, the DMA-TMS led to an increase in the Ti content measured by RBS while maintaining a somewhat hydrophobic surface. This is consistent with the results shown in Figure 5, where the DMA-TMS helps promote TiCl<sub>4</sub> diffusion into the bulk of the polymer, likely by passivating -OH sites exposed on the polymer surface. Figure 5 also demonstrates an increase in Si concentration in the bulk of the PHS polymer and close to the polymer surface after treatment with DMA-TMS, suggesting that some TMS groups also diffuse into the polymer (especially closer to the interface, which may be less dense). Therefore, it may be possible to further tune the amount of Ti deposition inside the polymer and its spatial distribution by varying the DMA-TMS treatment time. Comparing RBS and WCA results in Figure 7 to those in Figure S5, ALD TiO<sub>2</sub> grows similarly on these polymers before and after EUV exposure. Note that more cycle numbers were evaluated with WCA compared to RBS due to the relatively more convenient nature of WCA analysis.

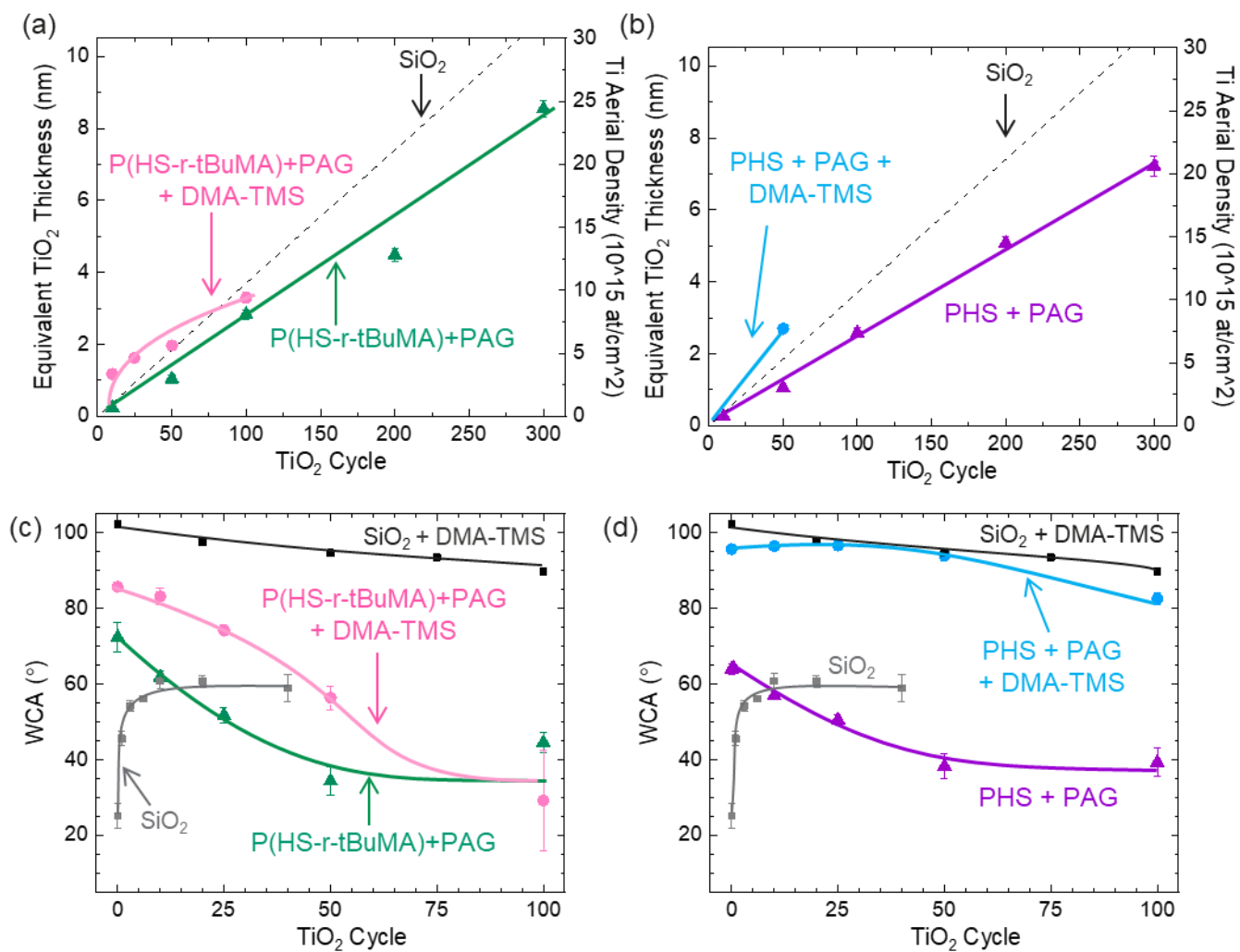


**Figure 7.** (a-b) RBS and (c-d) WCA measurements for various cycles of TiO<sub>2</sub> ALD on (a, c) P(HS-r-tBuMA) + PAG and (b, d) PHS + PAG. DMA-TMS treated and untreated data sets are indicated on the Figure. Data on DMA-TMS treated and untreated SiO<sub>2</sub> are shown as a reference, as indicated on the Figure. Lines are drawn as guides to the eye.

#### D. Selectivity of TiO<sub>2</sub> on Polymer Resists

The values for TiO<sub>2</sub> thickness (t) vs ALD cycle obtained from RBS data on SiO<sub>2</sub> and different polymers in Figure 3 and 7 can be used to quantify the extent of selectivity (S) for growth on SiO<sub>2</sub> vs polymer,

$$S_{SiO_2 \text{ v. polymer}} = \frac{(t_{SiO_2} - t_{polymer})}{(t_{SiO_2} + t_{polymer})} \quad \text{Equation 2}$$

and for growth on untreated vs DMA-TMS-treated polymers:

$$S_{polymer \text{ v. SiO}_2\text{-TMS}} = \frac{(t_{polymer} - t_{SiO_2\text{-TMS}})}{(t_{polymer} + t_{SiO_2\text{-TMS}})} \quad \text{Equation 3}$$

Materials that allow large values of  $S_{SiO_2 \text{ v. polymer}}$  (i.e. growth on SiO<sub>2</sub> with minimal growth on the resist) are attractive for tone inversion applications, whereas materials with large  $S_{polymer \text{ v. SiO}_2\text{-TMS}}$  are favorable for resist hardening.

Figure 8a and b show the calculated values for S plotted vs TiO<sub>2</sub> thickness on SiO<sub>2</sub>. For  $S_{SiO_2 \text{ v. polymer}}$  in Figure 8a, PCHMA demonstrates the highest selectivity with  $S_{SiO_2 \text{ v. PCHMA}} = 0.76$  after ~4 nm of TiO<sub>2</sub> (100 cycles) on SiO<sub>2</sub>. Continued ALD enables  $S_{SiO_2 \text{ v. PCHMA}} > 0.7$  after 7.4 nm (200 cycles) of TiO<sub>2</sub>. We note the initial decrease in selectivity during the first 10 ALD cycles, corresponding to relatively rapid TiO<sub>2</sub> growth during the initial cycles, followed by slower growth. This is attributed to diffusion of TiCl<sub>4</sub> through the thin polymer layer to react with residual OH sites on the SiO<sub>2</sub> substrate (i.e. sites remaining after the HMDS prime and polymer spin-coating or due to lower polymer density at the substrate interface), as shown in Scheme S1.<sup>40,46</sup> After site consumption, Ti uptake is slow, with minimal growth for ~100 cycles. For the other polymers studied (i.e. without CHMA), selectivity decreases rapidly within the first 1-2 nm of

deposition on the SiO<sub>2</sub> growth surface. These results demonstrate that TiO<sub>2</sub> is inhibited on polymers with the cyclohexyl protecting group, making this structure a good candidate for tone inversion, as shown in Figure 1b. Further investigation should be conducted to minimize possible interactions between the TiCl<sub>4</sub> precursor and the underlying substrate beneath the polymer layer.

For  $S_{polymer \ v. \ SiO_2-TMS}$  in Figure 8b both PHS + PAG and P(HS-r-tBuMA) + PAG show  $S_{polymer \ v. \ SiO_2-TMS} = 0.90$  after ~4 nm of TiO<sub>2</sub>. This high selectivity is maintained in both the case of TiO<sub>2</sub> deposition on the as-spun polymers and for TiO<sub>2</sub> infiltration into DMA-TMS treated polymers. Because TiO<sub>2</sub> deposits equally well on both EUV exposed and unexposed surfaces, this resist hardening process could work with both positive and negative-tone resist materials.

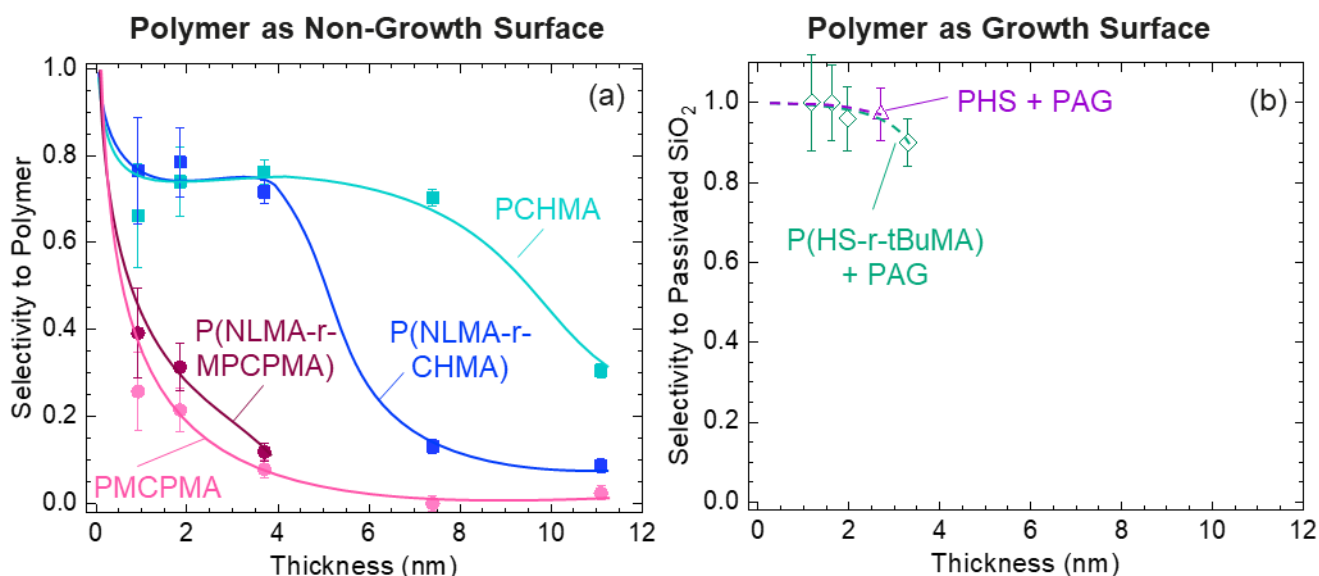


**Figure 8.** Selectivity as a function of deposited TiO<sub>2</sub> film thickness using (a) polymers as the non-growth surface (with SiO<sub>2</sub> as the growth surface) and (b) polymers as the growth surface (with DMA-TMS passivated SiO<sub>2</sub> as the non-growth surface). Lines are drawn as guides to the eye.

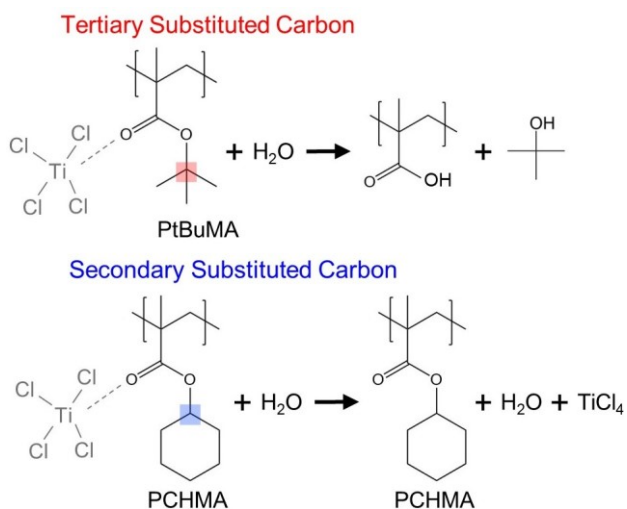
#### E. Mechanisms for Selectivity and Selectivity Loss

The differences in TiO<sub>2</sub> growth behavior are attributed to the small size and high Lewis acid character of the TiCl<sub>4</sub> precursor. The small molecular size facilitates diffusion into the bulk polymer during ALD to enable growth within the polymer,<sup>46,63</sup> as supported by TEM EDS (Fig. 5) and ToF-SIMS (Fig. S6). Previous reports indicate that diffusion is more significant for thinner polymers.<sup>40,46</sup> Additionally, from Figures 4, 5, and 7, polymers with a higher density of surface reactive sites (e.g. OH groups on PHS) facilitate TiCl<sub>4</sub> reaction at the surface, thus decreasing the extent of sub-surface diffusion, consistent with previous reports.<sup>41,64,65</sup> In contrast, when there are few reactive sites on the polymer surface (i.e. EUV unexposed PtBuMA or DMA-TMS passivated PHS), then the TiCl<sub>4</sub> precursor is more likely to diffuse into the bulk polymer and react sub-surface.<sup>41,64,65</sup> The sub-surface infiltration of Ti-species provides a potential method to increase etch resistance without significantly affecting CD, consistent with previous results.<sup>26</sup> Accordingly, tuning the surface species (e.g. with the DMA-TMS inhibitor or various protecting groups) provides a viable method to control Ti-species placement on the surface vs within the bulk of the polymer film. For example, diffusion could be further reduced using bulkier ALD precursors, bulkier polymer backbones, or longer DMA-TMS passivation times.<sup>46</sup> Note that it could also be possible for some sub-surface TiO<sub>2</sub> to inhibit further diffusion of Ti-species.

We note that while polymer glass transition temperature ( $T_g$ ) is an important factor for EUV resists and polymer processing, the  $T_g$  does not have a clear impact on growth rate for polymers studied here. Typically, more mobile chains (i.e. lower  $T_g$ ) are expected to enhance diffusion and thus result in more Ti uptake.<sup>66</sup> However, in this work, a similar Ti growth rate is observed on PHS ( $T_g \sim 150$  °C),<sup>66</sup> P(HS-r-tBuMA) ( $T_g \sim 98$  °C),<sup>19</sup> and PMCPMA ( $T_g \sim 79$  °C)<sup>19</sup> despite different  $T_g$  values reported in literature, which may be attributed to changes in actual  $T_g$  values due to

influences from resist thickness, copolymer constituents, PAG, EUV exposure, and the underlying substrate.<sup>17,56,66</sup>

Another mechanism for selectivity loss in this work is attributed to coordination between the Lewis acidic  $\text{TiCl}_4$  precursor and the lone electron pair in the carbonyl bond of acrylates,<sup>46,63,67</sup> as shown in Scheme 2. This could explain the smaller WCAs after  $\text{TiO}_2$  deposition on polymers than the average  $\text{TiO}_2$  WCA (Fig. 3 and 7). While alternative Ti precursors that are weaker Lewis acids could be used to mitigate this undesired reaction,<sup>46</sup>  $\text{TiCl}_4$  is necessitated in this case by the low thermal budget for polymer processing. An alternative solution is the use of polymers with a secondary carbon bound to the ester group (e.g. the cyclohexyl group), which is less susceptible to Lewis acid reaction than a tertiary carbon (e.g. *tert*-butyl and methylcyclopentyl groups, Scheme 2). Indeed, results in Figure 3 demonstrate significantly less  $\text{TiO}_2$  on polymers with the cyclohexyl protecting group (i.e. PCHMA and P(NLMA-r-CHMA)) compared to polymers with tertiary carbons (i.e. polymers containing tBuMA or MCPMA). In each case,  $\text{TiCl}_4$  may coordinate with the carbonyl group in the methacrylate backbone, but the subsequent hydrolysis reaction is more likely to occur with the tertiary substituted protecting group compared to the less stable, secondary substituted carbon in the protecting group. Therefore, we conclude that deposition during  $\text{TiO}_2$  ALD on the methacrylate polymers containing a tertiary carbon on the ester group is related to Lewis acid catalyzed reactions between the  $\text{TiCl}_4$  precursor and methacrylate polymers. Selectivity to the polymer can thus be enabled by tuning the structure of the resist material to reduce these reactions, for example with the cyclohexyl protecting group studied here.



**Scheme 2.** Proposed reaction mechanisms between  $\text{TiCl}_4$ ,  $\text{H}_2\text{O}$ , and methacrylate polymers with tertiary vs secondary substituted carbon linking the protecting group to ester group.

## CONCLUSION

In this work, we successfully demonstrate the compatibility of  $\text{TiO}_2$  ASD with several polymethacrylate-based thin EUV resist materials for potential use in both tone inverting and resist hardening applications. PCHMA, with its secondary carbon linking the protecting and ester groups, succeeds in inhibiting  $\text{TiO}_2$  deposition by reducing reactions catalyzed by the  $\text{TiCl}_4$  Lewis acid, whereas polymers with a tertiary carbon adjacent to the ester group are prone to reactions catalyzed by Lewis acids and therefore enable  $\text{TiO}_2$  deposition regardless of the protecting group size. PCHMA inhibits  $\text{TiO}_2$  growth up to  $\sim 200$  cycles, making this a promising structure to utilize in resist candidates for tone inversion applications (e.g. on oxide underlayers). On the other hand,  $\text{TiO}_2$  is successfully deposited on P(HS-r-tBuMA) and PHS resist materials regardless of the presence of PAG or EUV exposure, and thus these materials are of interest for resist hardening applications. We furthermore demonstrate that the resist material processing is compatible with a DMA-TMS inhibitor. The DMA-TMS treatment inhibits growth on  $\text{SiO}_2$ , for example, while

enabling Ti infiltration into the bulk resist, thus providing a means for resist hardening via infiltration. Further investigation is required to minimize resist swelling due to diffusion of the DMA-TMS inhibitor and/or Ti-species and enable increased resist etch resistance without significantly affecting CDs. We expect these findings are highly relevant to tune and design polymer structures for EUV lithography and will lead to increased integration between ASD and EUV resists to enable enhanced patterning resolution for advanced devices. Future work should focus on extending these ASD results to additional resist structures and to nanopatterns.

## ASSOCIATED CONTENT

**Supporting Information.** See the supplementary material for data related to XPS, WCA, AFM, RBS, ToF-SIMS, and TEM + EDS, as well as the structure of the PAG.

The following files are available free of charge.

Supporting Information (PDF)

## AUTHOR INFORMATION

### **Corresponding Author**

\*Annelies Delabie. \* Please address all correspondence to [Annelies.Delabie@imec.be](mailto:Annelies.Delabie@imec.be).

### **Author Contributions**

The manuscript was written through contributions of all authors. All authors have given approval to the final version of the manuscript.

### **Notes**

The authors have no conflicts of interest to declare.

## ACKNOWLEDGMENT

The authors would like to thank Nadia Vandebroek for her insightful discussions and material processing. The authors would also like to acknowledge Ilse Hoflijk, Thierry Conard, Johan

Desmet, and Johan Meersschaut (imec, Belgium) for their discussions involving XPS and RBS characterization and data analysis.

## ABBREVIATIONS

AFM, atomic force microscopy; ALD, atomic layer deposition; ASD, area-selective deposition; EDS, energy dispersive spectroscopy; EUV, extreme ultra-violet; NLMA, 2-oxohexahydro-6aH-3,5-methanocyclopenta[b]furan-6a-yl 2,2-dimethylbutanoate; PAG, photo-acid generator; PCHMA, poly(cyclohexyl methacrylate); PHS, poly(p-hydroxystyrene); PMCPMA, poly(1-methylcyclopentyl methacrylate); PtBuMA, poly(tert-butyl methacrylate); RBS, Rutherford backscattering spectrometry; TEM, transmission electron microscopy; ToF-SIMS, time of flight-secondary ion mass spectrometry; WCA, water contact angle; XPS, x-ray photoelectron.

## REFERENCES

- (1) Moore, G. E. Cramming More Components onto Integrated Circuits. *Electronics (Basel)* **1965**, 38 (8).
- (2) Waldrop, M. M. The Chips Are down for Moore's Law: Nature News & Comment. 2016.
- (3) Li, L.; Liu, X.; Pal, S.; Wang, S.; Ober, C. K.; Giannelis, E. P. Extreme Ultraviolet Resist Materials for Sub-7 Nm Patterning. *Chem. Soc. Rev.* **2017**, 46, 4855–4866.
- (4) Lin, B. J. Making Lithography Work for the 7-Nm Node and beyond in Overlay Accuracy, Resolution, Defect, and Cost. *Microelectron Eng* **2015**, 143, 91–101.
- (5) Wu, B.; Kumar, A. Extreme Ultraviolet Lithography and Three Dimensional Integrated Circuit—A Review. *Appl Phys Rev* **2014**, 1 (1), 011104.
- (6) Clark, R.; Tapily, K.; Yu, K.-H.; Hakamata, T.; Consiglio, S.; O'Meara, D.; Wajda, C.; Smith, J.; Leusink, G. Perspective: New Process Technologies Required for Future Devices and Scaling. *APL Mater* **2018**, 6 (5), 058203.
- (7) Schuegraf, K.; Abraham, M. C.; Brand, A.; Naik, M.; Thakur, R. Semiconductor Logic Technology Innovation to Achieve Sub-10 Nm Manufacturing. *IEEE Journal of the Electron Devices Society* **2013**, 1 (3), 66–75.
- (8) Gwyn, C. W.; Stulen, R.; Sweeney, D.; Attwood, D. Extreme Ultraviolet Lithography. *Journal of Vacuum Science & Technology B* **1998**, 16 (6), 3142.

- (9) Klein, M. v.; Furtak, T. E. *Optics*, 2nd ed.; Wiley, 1991.
- (10) Cardineau, B.; del Re, R.; Marnell, M.; Al-Mashat, H.; Vockenhuber, M.; Ekinici, Y.; Sarma, C.; Freedman, D. A.; Brainard, R. L. Photolithographic Properties of Tin-Oxo Clusters Using Extreme Ultraviolet Light (13.5 Nm). *Microelectron Eng* **2014**, *127*, 44–50.
- (11) Ober, C. K.; Xu, H.; Kosma, V.; Sakai, K.; Giannelis, E. P. EUV Photolithography: Resist Progress and Challenges. In *Proc. SPIE*; SPIE, 2018; Vol. 10583, p 1058306.
- (12) Kasahara, K.; Xu, H.; Kosma, V.; Odent, J.; Giannelis, E. P.; Ober, C. K. Nanoparticle Photoresist Studies for EUV Lithography. *Extreme Ultraviolet (EUV) Lithography VIII* **2017**, *10143*, 1014308.
- (13) Higgins, C. D.; Szmanda, C. R.; Antohe, A.; Denbeaux, G.; Georger, J.; Brainard, R. L. Resolution, Line-Edge Roughness, Sensitivity Tradeoff, and Quantum Yield of High Photo Acid Generator Resists for Extreme Ultraviolet Lithography. *Jpn J Appl Phys* **2011**, *50* (036504).
- (14) Mojarad, N.; Gobrecht, J.; Ekinici, Y. Beyond EUV Lithography: A Comparative Study of Efficient Photoresists' Performance. *Sci Rep* **2015**, *5* (9235).
- (15) Fujimori, T.; Tsuchihashi, T.; Itani, T. Recent Progress of Negative-Tone Imaging Process and Materials with EUV Exposure. In *Proc. SPIE*; 2015; Vol. 9425, p 942505.
- (16) Wu, B.; Kumar, A. Extreme Ultraviolet Lithography: A Review. *Journal of Vacuum Science & Technology B* **2007**, *25* (6), 1743.
- (17) Severi, J.; de Simone, D.; de Gendt, S. Dielectric Response Spectroscopy as Means to Investigate Interfacial Effects for Ultra-Thin Film Polymer-Based High NA EUV Lithography. *Polymers (Basel)* **2020**, *12* (12), 2971.
- (18) Itani, T.; Kozawa, T. Resist Materials and Processes for Extreme Ultraviolet Lithography. *Jpn J Appl Phys* **2012**, *52* (1R), 010002.
- (19) Enomoto, S.; Kozawa, T. Study of Electron-Beam and Extreme-Ultraviolet Resist Utilizing Polarity Change and Radical Crosslinking. *Journal of Vacuum Science & Technology B* **2018**, *36* (3), 031601.
- (20) Kozawa, T.; Santillan, J. J.; Itani, T. Feasibility Study of Sub-10-Nm-Half-Pitch Fabrication by Chemically Amplified Resist Processes of Extreme Ultraviolet Lithography: II. Stochastic Effects. *Jpn J Appl Phys* **2015**, *54* (3), 036507.
- (21) Guen-Ho Hwang, al; Patil, M.; Seo, S.-K.; Yu, C.-B.; Hur, I.-B.; Hyun Kim, D.; Shin, C.; Jung, S.-M.; Lee, Y.-H.; Choi, S.-S.; et al. Patterning Capability and Limitations by Pattern Collapse in 45nm and below Node Photo Mask Production. In *Proc. SPIE*; SPIE, 2008; Vol. 7028, p 702824.
- (22) Lugier, O.; Thakur, N.; Wu, L.; Vockenhuber, M.; Ekinici, Y.; Castellanos, S. Bottom-Up Nanofabrication with Extreme-Ultraviolet Light: Metal–Organic Frameworks on Patterned Monolayers. *ACS Appl Mater Interfaces* **2021**, *13*, 43777–43786.

- (23) Goldfarb, D. L.; Bruce, R. L.; Bucchignano, J. J.; Klaus, D. P.; Guillorn, M. A.; Wu, C. J. Pattern Collapse Mitigation Strategies for EUV Lithography. In *Proc. SPIE*; SPIE, 2012; Vol. 8322, p 832205.
- (24) Krysak, M.; Trikeriotis, M.; Schwartz, E.; Lafferty, N.; Xie, P.; Marie Krysak, al; Smith, B.; Zimmerman, P.; Montgomery, W.; Giannelis, E.; et al. Development of an Inorganic Nanoparticle Photoresist for EUV, e-Beam, and 193nm Lithography. <https://doi.org/10.1117/12.879385> **2011**, 7972 (15), 408–413.
- (25) Gokan, H.; Esho, S.; Ohnishi, Y. Dry Etch Resistance of Organic Materials. *J Electrochem Soc* **1983**, 130 (1), 143–146.
- (26) Tseng, Y. C.; Peng, Q.; Ocola, L. E.; Czaplewski, D. A.; Elam, J. W.; Darling, S. B. Enhanced Polymeric Lithography Resists via Sequential Infiltration Synthesis. *J Mater Chem* **2011**, 21 (32), 11722–11725.
- (27) Jablonski, E. L.; Prabhu, V. M.; Sambasivan, S.; Fischer, D. A.; Lin, E. K.; Goldfarb, D. L.; Angelopoulos, M.; Ito, H. Surface and Bulk Chemistry of Chemically Amplified Photoresists: Segregation in Thin Films and Environmental Stability Issues. In *Proc. SPIE*; SPIE, 2004; Vol. 5376.
- (28) Vanelderden, P.; de Simone, D.; Spampinato, V.; Franquet, A.; Vandenberghe, G. The Role of Underlayers in EUVL. *Journal of Photopolymer Science and Technology* **2018**, 31 (2), 209–214.
- (29) Nye, R. A.; Kelliher, A. P.; Gaskins, J. T.; Hopkins, P. E.; Parsons, G. N. Understanding Molecular Layer Deposition Growth Mechanisms in Polyurea via Picosecond Acoustics Analysis. *Chemistry of Materials* **2020**, 32 (4), 1553–1563.
- (30) Nye, R. A.; Dongen, K. Van; Oka, H.; Furutani, H.; Parsons, G.; Simone, D. De; Delabie, A. Improving Polymethacrylate EUV Resists with TiO<sub>2</sub> Area-Selective Deposition. In *Proc. SPIE*; SPIE, 2022; Vol. 12055, p 120550C.
- (31) Grillo, F.; Soethoudt, J.; Marques, E. A.; de Martín, L.; van Dongen, K.; Ruud Van Ommen, J.; Delabie, A. Area-Selective Deposition of Ruthenium by Area-Dependent Surface Diffusion. *Chemistry of Materials* **2020**, 32 (22), 9560–9572.
- (32) Song, S. K.; Saare, H.; Parsons, G. N. Integrated Isothermal Atomic Layer Deposition/Atomic Layer Etching Supercycles for Area-Selective Deposition of TiO<sub>2</sub>. *Chemistry of Materials* **2019**, 31 (13), 4793–4804.
- (33) Parsons, G. N.; Clark, R. D. Area-Selective Deposition: Fundamentals, Applications, and Future Outlook. *Chemistry of Materials* **2020**, 32 (12), 4920–4953.
- (34) de Simone, D.; Vesters, Y.; Vandenberghe, G. Photoresists in Extreme Ultraviolet Lithography (EUVL). *Advanced Optical Technologies* **2017**, 6 (3–4), 163–172.
- (35) Tsubaki, H.; Nihashi, W.; Tsuchihashi, T.; Yamamoto, K.; Goto, T. Negative-Tone Imaging with EUV Exposure toward 13nm Hp. In *Proc. SPIE*; 2016; Vol. 9776, p 977608.

- (36) Soethoudt, J.; Tomczak, Y.; Meynaerts, B.; Chan, B. T.; Delabie, A. Insight into Selective Surface Reactions of Dimethylamino-Trimethylsilane for Area-Selective Deposition of Metal, Nitride, and Oxide. *Journal of Physical Chemistry C* **2020**, *124* (13), 7163–7173.
- (37) Wojtecki, R.; Ma, J.; Cordova, I.; Arellano, N.; Lioni, K.; Magbitang, T.; Pattison, T. G.; Zhao, X.; Delenia, E.; Lanzillo, N.; et al. Additive Lithography–Organic Monolayer Patterning Coupled with an Area-Selective Deposition. *ACS Appl Mater Interfaces* **2021**, *13* (7), 9081–9090.
- (38) Lutker-Lee, K.; Church, J.; Miller, E.; Raley, A.; Meli, L. Plasma-Based Area Selective Deposition for Extreme Ultraviolet Resist Defectivity Reduction and Process Window Improvement. *Journal of Vacuum Science & Technology B* **2022**, *40* (3), 032204.
- (39) Hill, G. T.; Lee, D. T.; Williams, P. S.; Needham, C. D.; Dandley, E. C.; Oldham, C. J.; Parsons, G. N. Insight on the Sequential Vapor Infiltration Mechanisms of Trimethylaluminum with Poly(Methyl Methacrylate), Poly(Vinylpyrrolidone), and Poly(Acrylic Acid). *The Journal of Physical Chemistry C* **2019**, *123* (26), 16146–16152.
- (40) Sinha, A.; Hess, D. W.; Henderson, C. L. Area-Selective ALD of Titanium Dioxide Using Lithographically Defined Poly(Methyl Methacrylate) Films. *J Electrochem Soc* **2006**, *153* (5), G465.
- (41) Parsons, G. N.; Atanasov, S. E.; Dandley, E. C.; Devine, C. K.; Gong, B.; Jur, J. S.; Lee, K.; Oldham, C. J.; Peng, Q.; Spagnola, J. C.; et al. Mechanisms and Reactions during Atomic Layer Deposition on Polymers. *Coord Chem Rev* **2013**, *257*, 3323–3331.
- (42) Yao, H.; Mullen, S.; Wolfer, E.; Mckenzie, D.; Dioses, A.; Rahman, D.; Cho, J.; Padmanaban, M.; Petermann, C.; Hong, S.; et al. Spin-on Metal Oxides and Their Applications for Next Generation Lithography. *Journal of Photopolymer Science and Technology* **2016**, *29* (1), 59–67.
- (43) Soethoudt, J.; Hody, H.; Spampinato, V.; Franquet, A.; Briggs, B.; Chan, B. T.; Delabie, A. Defect Mitigation in Area-Selective Atomic Layer Deposition of Ruthenium on Titanium Nitride/Dielectric Nanopatterns. *Adv Mater Interfaces* **2019**, *6* (20), 1900896.
- (44) Soethoudt, J.; Crahaij, S.; Conard, T.; Delabie, A. Impact of SiO<sub>2</sub> Surface Composition on Trimethylsilane Passivation for Area-Selective Deposition. *J Mater Chem C Mater* **2019**, *7* (38), 11911–11918.
- (45) Nye, R. A.; Song, S. K.; Dongen, K. van; Delabie, A.; Parsons, G. N. Mechanisms for Undesired Nucleation on H-Terminated Si and Dimethylamino-Trimethylsilane Passivated SiO<sub>2</sub> during TiO<sub>2</sub> Area-Selective Atomic Layer Deposition. *Appl Phys Lett* **2022**, *121* (8), 082102.
- (46) Sinha, A.; Hess, D. W.; Henderson, C. L. Area Selective Atomic Layer Deposition of Titanium Dioxide: Effect of Precursor Chemistry. *Journal of Vacuum Science & Technology B* **2006**, *24* (6), 2523.

- (47) Färm, E.; Kemell, M.; Santala, E.; Ritala, M.; Leskelä, M. Selective-Area Atomic Layer Deposition Using Poly(Vinyl Pyrrolidone) as a Passivation Layer. *J Electrochem Soc* **2010**, *157* (1), K10.
- (48) Kemell, M.; Färm, E.; Ritala, M.; Leskelä, M. Surface Modification of Thermoplastics by Atomic Layer Deposition of Al<sub>2</sub>O<sub>3</sub> and TiO<sub>2</sub> Thin Films. *Eur Polym J* **2008**, *44* (11), 3564–3570.
- (49) Färm, E.; Kemell, M.; Ritala, M.; Leskelä, M. Selective-Area Atomic Layer Deposition Using Poly(Methyl Methacrylate) Films as Mask Layers. *Journal of Physical Chemistry C* **2008**, *112* (40), 15791–15795.
- (50) Stevens, E.; Tomczak, Y.; Chan, B. T.; Sanchez, A.; Parsons, G. N.; Delabie, A.; Leuven, K. Area-Selective Atomic Layer Deposition of TiN, TiO<sub>2</sub>, and HfO<sub>2</sub> on Silicon Nitride with Inhibition on Amorphous Carbon. *Chemistry of Materials* **2018**, *30*, 3223–3232.
- (51) Park, M. H.; Jang, Y. J.; Sung-Suh, H. M.; Sung, M. M. Selective Atomic Layer Deposition of Titanium Oxide on Patterned Self-Assembled Monolayers Formed by Microcontact Printing. *Langmuir* **2004**, *20* (6), 2257–2260.
- (52) Saare, H.; Song, S. K.; Kim, J.-S.; Parsons, G. N. Effect of Reactant Dosing on Selectivity during Area-Selective Deposition of TiO<sub>2</sub> via Integrated Atomic Layer Deposition and Atomic Layer Etching. *J Appl Phys* **2020**, *128* (10), 105302.
- (53) Khan, R.; Shong, B.; Ko, B. G.; Lee, J. K.; Lee, H.; Park, J. Y.; Oh, I. K.; Raya, S. S.; Hong, H. M.; Chung, K. B.; et al. Area-Selective Atomic Layer Deposition Using Si Precursors as Inhibitors. *Chemistry of Materials* **2018**, *30* (21), 7603–7610.
- (54) Nye, R. A.; Dongen, K. van; Oka, H.; Simone, D. de; Parsons, G. N.; Delabie, A. Compatibility between Polymethacrylate-Based Extreme Ultraviolet Resists and TiO<sub>2</sub> Area-Selective Deposition. *JM3* **2022**, *21* (4), 041407.
- (55) Sinha, A.; Hess, D. W.; Henderson, C. L. A Top Surface Imaging Method Using Area Selective ALD on Chemically Amplified Polymer Photoresist Films. *Electrochemical and Solid-State Letters* **2006**, *9* (11), G330–G333.
- (56) Shin, H. S.; Jung, Y. M.; Lee, J.; Chang, T.; Ozaki, Y.; Kim, S. bin. Structural Comparison of Langmuir-Blodgett and Spin-Coated Films of Poly(Tert-Butyl Methacrylate) by External Reflection FTIR Spectroscopy and Two-Dimensional Correlation Analysis. *Langmuir* **2002**, *18* (14), 5523–5528.
- (57) Nye, R. A.; Dongen, K. van; Oka, H.; Furutani, H.; Parsons, G.; Simone, D. de; Delabie, A. Improving Polymethacrylate EUV Resists with TiO<sub>2</sub> Area-Selective Deposition. *Proc SPIE* **2022**, *12055* (120550C).
- (58) Grzeskowiak, S.; Denbeaux, G. H.; Brainard, R. L.; Kaminsky, J.; Murphy, M.; Gibbons, S.; Chandonait, J. Polymer Effects on PAG Acid Yield in EUV Resists. <https://doi.org/10.1117/12.2297692> **2018**, *10586*, 27–33.

- (59) Yarbrough, J.; Shearer, A. B.; Bent, S. F. Next Generation Nanopatterning Using Small Molecule Inhibitors for Area-Selective Atomic Layer Deposition. *Journal of Vacuum Science & Technology A* **2021**, *39* (2), 021002.
- (60) Atanasov, S. E.; Kalanyan, B.; Parsons, G. N. Inherent Substrate-Dependent Growth Initiation and Selective-Area Atomic Layer Deposition of TiO<sub>2</sub> Using “Water-Free” Metal-Halide/Metal Alkoxide Reactants. *Journal of Vacuum Science & Technology A* **2016**, *34* (1), 01A148.
- (61) Kim, S. K.; Hoffmann-Eifert, S.; Reiners, M.; Waser, R. Relation Between Enhancement in Growth and Thickness-Dependent Crystallization in ALD TiO<sub>2</sub> Thin Films. *J Electrochem Soc* **2011**, *158* (1), D6.
- (62) Chen, R.; Kim, H.; McIntyre, P. C.; Bent, S. F. Investigation of Self-Assembled Monolayer Resists for Hafnium Dioxide Atomic Layer Deposition. *Chemistry of Materials* **2005**, *17* (3), 536–544.
- (63) Dandley, E. C.; Needham, C. D.; Williams, P. S.; Brozena, A. H.; Oldham, C. J.; Parsons, G. N. Temperature-Dependent Reaction between Trimethylaluminum and Poly(Methyl Methacrylate) during Sequential Vapor Infiltration: Experimental and Ab Initio Analysis. *J Mater Chem C Mater* **2014**, *2* (44), 9416–9424.
- (64) Brozena, A. H.; Oldham, C. J.; Parsons, G. N. Atomic Layer Deposition on Polymer Fibers and Fabrics for Multifunctional and Electronic Textiles. *Journal of Vacuum Science & Technology A* **2016**, *34* (1), 010801.
- (65) Parsons, G. N. Atomic Layer Deposition on Soft Materials. In *Atomic Layer Deposition of Nanostructured Materials*; John Wiley & Sons, Ltd, 2012; pp 271–300.
- (66) de Silva, A.; Felix, N.; Sha, J.; Lee, J.-K.; Ober, C. K. Molecular Glass Resists for next Generation Lithography. In *Proc. SPIE*; SPIE, 2008; Vol. 6923, p 69231L.
- (67) Klement, P.; Anders, D.; Gumbel, L.; Bastianello, M.; Michel, F.; Schörmann, J.; Elm, M. T.; Heiliger, C.; Chatterjee, S. Surface Diffusion Control Enables Tailored-Aspect-Ratio Nanostructures in Area-Selective Atomic Layer Deposition. *ACS Appl Mater Interfaces* **2021**, *13* (16), 19398–19405.

## BRIEFS

Area-selective deposition of TiO<sub>2</sub> on polymethacrylate EUV resists demonstrates potential for resist hardening and tone inversion applications for higher resolution pattern transfer.

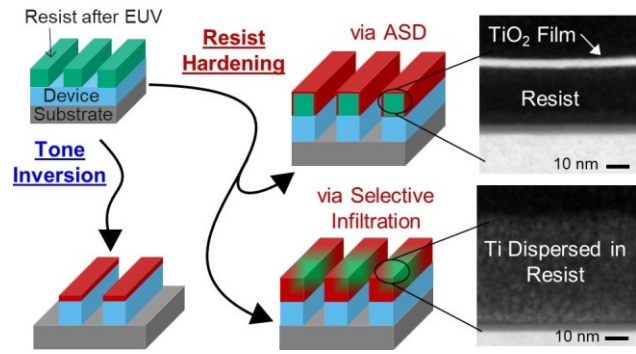


**Table of Contents Figure.**